

Targeting Ligand Independent Tropism of siRNA-LNP by Small Molecules for Directed Therapy of Liver or Myeloid Immune Cells

Cheng Lin, Asmaa Mostafa, Alexander Jans, Justina Clarinda Wolters, Mohamed Ramadan Mohamed, Emiel P. C. Van der Vorst, Christian Trautwein, and Matthias Bartneck*

Hepatic clearance of lipid nanoparticles (LNP) with encapsulated nucleic acids restricts their therapeutic applicability. Therefore, tools for regulating hepatic clearance are of high interest for nucleic acid delivery. To this end, this work employs wild-type (WT) and low-density lipoprotein receptor (*Ldlr*^{-/-}) mice pretreated with either a leukotriene B4 receptor inhibitor (BLT1i) or a high-density lipoprotein receptor inhibitor (HDLRi) prior to the injection of siRNA-LNP. This work is able to demonstrate significantly increased hepatic uptake of siRNA-LNP by the BLT1i in *Ldlr*^{-/-} mice by in vivo imaging and discover an induction of specific uptake-related proteins. Irrespective of the inhibitors and *Ldlr* deficiency, the siRNA-LNP induced RNA-binding and transport-related proteins in liver, including haptoglobin (HP) that is also identified as most upregulated serum protein. This work observes a downregulation of proteins functioning in hepatic detoxification and of serum opsonins. Most strikingly, the HDLRi reduces hepatic uptake and increases siRNA accumulation in spleen and myeloid immune cells of blood and liver. RNA sequencing demonstrates leukocyte recruitment by the siRNA-LNP and the HDLRi through induction of chemokine ligands in liver tissue. The data provide insights into key mechanisms of siRNA-LNP biodistribution and indicate that the HDLRi has potential for extrahepatic and leukocyte targeting.

1. Introduction

RNA therapeutics have emerged as important tools in vaccinations of billions of people.^[1] Prior to the mRNA vaccines for COVID-19, the first siRNA-based drug called Onpatro (patisiran) received its approval for the treatment of hereditary transthyretin-mediated amyloidosis in 2018.^[2] Both siRNA and mRNA therapeutics rely on lipid nanoparticle (LNP) technology to avoid degradation and to ensure intracellular delivery. Ionizable cationic lipids such as heptatriaconta-6,9,28,31-tetraen-19-yl-4-(dimethylamino) butanoate (MC3) are crucial LNP components that make up a large part of the lipid fraction of the particles.^[2] The siRNA-LNP are produced by rapidly mixing siRNA in buffer and lipids in organic solvents using microfluidic mixing leading to nanoparticle self-assembly. Following cellular uptake, the ionizable lipids of LNP induce endosomal escape of the RNA due to charge interactions of the lipids with the endosomal membrane.^[3]

C. Lin, A. Mostafa, A. Jans, M. R. Mohamed, C. Trautwein, M. Bartneck
Department of Internal Medicine III
University Hospital RWTH Aachen
Pauwelsstraße 30, 52074 Aachen, Germany
E-mail: mbartneck@ukaachen.de

C. Lin
Department of Rheumatology and Shanghai Institute of Rheumatology
Renji Hospital
School of Medicine
Shanghai Jiao Tong University
Shanghai, China


A. Mostafa
Department of Microbial Biotechnology
Biotechnology Research Institute
National Research Center
33 El-Bohouth St., El-Dokki, Giza 12622, Egypt

J. C. Wolters
Department of Pediatrics
Section Systems Medicine of Metabolism and Signaling
University of Groningen
University Medical Center Groningen
Groningen 9713 AV, The Netherlands

E. P. C. Van der Vorst
Interdisciplinary Center for Clinical Research (IZKF)
RWTH Aachen University
52074 Aachen, Germany

E. P. C. Van der Vorst
Institute for Molecular Cardiovascular Research (IMCAR)
RWTH Aachen University
52074 Aachen, Germany

E. P. C. Van der Vorst
Institute for Cardiovascular Prevention (IPEK)
Ludwig-Maximilians-University Munich
80336 Munich, Germany

 The ORCID identification number(s) for the author(s) of this article can be found under <https://doi.org/10.1002/adhm.202202670>

© 2023 The Authors. Advanced Healthcare Materials published by Wiley-VCH GmbH. This is an open access article under the terms of the Creative Commons Attribution License, which permits use, distribution and reproduction in any medium, provided the original work is properly cited.

DOI: 10.1002/adhm.202202670

It is well-known that siRNA-LNP accumulate in hepatocytes following intravenous administration. This is owed to an endogenous transport system of lipoprotein receptors and apolipoproteins.^[3] The lipoprotein receptors can be classified into two major groups: the first category are the endocytic receptors that bind the cargo via lipid-binding lipoproteins and include the LDLR, LDLR-associated proteins, and the type A scavenger receptors. The second category contains class B scavenger receptors such as the HDLR scavenger receptor B1 (SR-B1), SR-B2 and CD36.^[4] The most explored route for LNP transport in the body is based on Apolipoprotein E (APOE) that binds to the LNP and directs RNA-LNP to the LDLR that is strongly expressed by hepatocytes. Studies with *apoE*^{-/-} mice and *Ldlr*^{-/-} mice have demonstrated ligand and receptor dependence of LNP more than 10 years ago.^[3] Similar to the LDLR, the SR-B1 is mostly expressed by hepatocytes.^[5] The SR-B1 is, until now, the only identified HDLR.^[6] The HDLR inhibitor (HDLRi; also called block lipid transport 1) binds SR-B1 directly in the membrane environment as demonstrated in liposome-based binding assays.^[7]

The role of the immune system and related processes for intravenously administered RNA-LNP and other genetic medicines has received little attention in the past. Improved understanding of the interactions with the immune system might help to reduce or overcome the necessity of premedication of genetic medicines including Onpatro. Specific lipids and lipoproteins play important roles during inflammation and can dampen the severity of early stage inflammatory disease. However, if such changes are persistent they contribute to an increased risk of atherosclerosis.^[8] Little is known about the functions of lipoprotein receptors for uptake of RNA-LNP by leukocytes and the molecular mechanisms of this interrelation. The role of immune cells can be studied by an inhibition of leukocyte infiltration and phagocytosis that can for instance be achieved by inhibition of the leukotriene B4 receptor (BLT-1).^[9] The inhibitor U75302 binds to BLT-1 and attenuates inflammatory disease.^[10]

We have shown in previous studies that particularly the myeloid leukocytes in blood and liver (such as monocytes, macrophages, neutrophils, and dendritic cells (DC)) are highly efficient in the uptake of nanoparticles generated from gold, polymers, and lipids.^[11] Beneath these myeloid immune cells, the lymphoid immune cells such as CD3⁺ T cells, CD19⁺ B cells, and the CD56⁺ innate natural killer (NK) cells internalize significantly fewer amounts of nanoparticles than myeloid cells.^[11] The lymphoid T and B cells function in adaptive immunity and the T and NK cells further have the capability to selectively kill abnormal cells. Granulocytes (e.g., neutrophils) and monocytes are circulating phagocytes. Murine granulocytes are CD11b⁺Ly6G⁺ whereas monocytes are CD11b⁺Ly6G⁻ and can be further divided into functionally distinct subpopulations: inflammatory Ly6C^{high} monocytes that have migrated from the bone marrow into the blood and resident Ly6C^{low} monocytes that are mature and exhibit anti-inflammatory properties.^[11a] In the liver, one can distinguish different subsets of macrophages and DCs. The key populations of hepatic macrophages are defined as F4/80⁺CD11b⁺ monocyte-derived macrophages (MoMφ) that are continuously replenished from blood monocytes, and the stem cell-derived F4/80^{low}CD11b⁺ Kupffer cells (KC). There are also various different subsets of DC in the liver that among other markers can be distinguished based on their expression of MHCII and CD11c.^[12]

Various strategies have been explored to improve the delivery of therapeutic RNA to myeloid immune cells in the liver. A frequently performed strategy to enhance accumulation of nanoparticles in macrophages is based on coating the nanoparticles with mannose.^[13] Furthermore, selective targeting of Ly6C⁺ leukocytes in colitis has been achieved using LNP decorated with an antibody against Ly6C antigen delivering mRNA^[14] or siRNA.^[15] Moreover, Miettinen et al. have demonstrated that CD177-directed nanoparticles target neutrophils and are a useful tool to knock down genes in these cells.^[16] Recently, anionic RNA-LNPs were demonstrated to enhance their accumulation in hepatic endothelial cells and KC.^[17] Notably, also nontargeting LNPs were shown to target antigen-presenting cells (APC) in vivo,^[18] and neither the mRNA-based vaccines nor Onpatro are equipped with a targeting ligand.^[1]

The decoration of nanomedicines with specific ligands to encounter a specific tissue or cell type is an attractive concept. Hence, guiding the RNA-LNP to specific cells or tissues based on modulating lipid-associated processes would be a valuable tool. Here, we selected two small molecules, an inhibitor for the immune cell specific LTB4 (BLT1i), and one that mediates lipid transport into the liver by inactivating the HDLR (HDLRi) and that is expressed by hepatocytes. To study interrelations between liver and immune cells, we treated wild-type (WT) and *Ldlr*^{-/-} mice intravenously with the inhibitors prior to the administration of the siRNA-LNP in vivo. We performed an in-depth analysis of the biodistribution of the siRNA-LNP using noninvasive imaging and used flow cytometry to study changes in the immune cell counts. Flow cytometry was further used to quantify the accumulation of the siRNA-LNP in different leukocyte subsets. In order to gain improved understanding of the underlying molecular processes of siRNA-LNP biodistribution, we performed proteomics analysis of liver tissue and serum. RNA sequencing of liver tissue was done to explore the way of action of the HDLRi. We discovered several proteins being regulated by the siRNA-LNP. RNA sequencing of liver tissue among others confirmed the induction of transport-related proteins in liver tissue.

2. Results

2.1. Inhibition of the Leukotriene B4 Receptor Leads to Hepatic Accumulation of siRNA-LNP

The role of leukocytes for the biodistribution of siRNA-LNP remains poorly understood. We therefore generated three different types of siRNA-LNP based on the experimental requirements: the first type included a Cy 7 labeled carboxylic acid that enables the siRNA-LNP to be traced using non-invasive 3D FLT imaging, the second type included an siRNA with a label that can be quantified by flow cytometry, and the third one included an siRNA without any label. The siRNA-LNPs were characterized for their size using DLS, their charge was determined by zeta potential measurements, and the EE of siRNA was assessed by a Ribogreen assay. The sizes, charges, and EE of the different compositions were similar and hence the siRNA-LNPs were used interchangeably (Table 1).

We first wanted to address the impact of the leukotriene B4 receptor inhibitor (BLT1i) on the biodistribution of siRNA-LNP. Due to the well-known role of LDLR in the distribution of siRNA-

Table 1. Characterization of siRNA-LNP (lipid nanoparticles).

Carrier type	Medium	Size [nm]	Zetapotential [mV]	Encapsulation efficiency [%]
Cy7-siRNA-LNP	PBS	109.28 ± 16.87	0.97 ± 0.28	91.2 ± 2.3%
AF647-siRNA-LNP	PBS	93.62 ± 1.07	−5.49 ± 1.27	88.3 ± 4.1%
siRNA-LNP	PBS	89.74 ± 4.89	1.13 ± 0.51	93.6 ± 3.8%

siRNA-LNP were generated using a NanoAssemblr Spark and the size and zeta potential were measured.

LNP,^[3] we also integrated *Ldlr*^{−/−} mice into the experiment. We first pretreated some mice for 24 h with the BLT1i at 1 mg kg^{−1} so that the inhibitor could take its effect. Afterwards, the mice received the Cy7-labeled siRNA-LNP (Figure 1A). We observed an increased fluorescent signal in CT-FLT imaging in the *Ldlr*^{−/−} mice that received the BLT1i (Figure 1B). Quantifications of the signal showed that the signal increase was statistically significant after 24 h (Figure 1C). Ex vivo scans based on fluorescence reflectance imaging (FRI) of excised livers confirmed this accumulation (Figure 1D) and quantifications confirmed statistical significance of the hepatic accumulation after 24 h (Figure 1E). Immunofluorescence microscopy confirmed the distribution pattern in liver tissue (Figure S1, Supporting Information). Importantly, we have to point out that we noted an increased mortality after BLT1i treatment of the WT mice and therefore we stopped the experiments with this inhibitor.

The most interesting finding was the induction of hepatic uptake in the BLT1i-*Ldlr*^{−/−} group. Therefore, proteomics analyses of liver tissue were the next step to identify the molecular processes (Figure S2, Supporting Information). VENN diagrams reflect the regulation of proteins by the different conditions (Figure S3, Supporting Information). Protein enrichment showed that the most-enriched term of the upregulated proteins in the BLT1i-*Ldlr*^{−/−} group was the denotation “transport” (highlighted in red on top of the inner ring) (Figure 1F). Strikingly, the BLT1i-*Ldlr*^{−/−} group included 58 transport proteins that were upregulated—similar to the 56 in the WT group. The other groups included 19 to 41 proteins from the category transport (Table S2, Supporting Information). The Volcano plot of the BLT1i-*Ldlr*^{−/−} compared to untreated WT liver tissue illustrates regulation and significance of proteins with the three highlighted transport proteins: C-type lectin domain family 13 member A (CD302), Epidermal growth factor receptor (EGFR), and sterol carrier protein 2 (SCP2) (Figure 1G). These three proteins were linked to phagocytosis (CD302), and transport processes (EGFR, SCP2) (Figure 1H). Additional proteins induced in the BLT1i-*Ldlr*^{−/−} group, cytochrome P450 2D9 (CYP2D9), and inositol-3-phosphate synthase 1 (ISYNA1), have a function in lipid metabolism and likely contribute to the degradation and excretion of the siRNA-LNP from the body via hepatic clearance. These and other significantly upregulated liver proteins are provided in Table 2. A combined heatmap illustrates the 20 most upregulated liver proteins of each experimental group and compares their regulation to the other groups (Figure S4, Supporting Information).

These experiments show that leukocytes play an important role for the biodistribution of the siRNA-LNP.

2.2. siRNA-LNP Induce Upregulation of Proteins Involved in RNA Binding and Transport

Subsequently, we aimed to increase our understanding of the general effects of the siRNA-LNP on the liver and serum proteome, irrespective of the BLT1 inhibitor or genetic deficiency of *Ldlr*. We were interested to see which proteins were enriched in liver tissue and hence generated Volcano plots to study the effects of the siRNA-LNP on the hepatic proteome in WT mice (Figure 2A). We found that interferon-induced protein with tetratricopeptide repeats 1 (IFIT1) (19- to 52-fold upregulation) and ubiquitin-like modifier (ISG15) (13- to 25-fold upregulation) were most upregulated of all annotated liver proteins under any experimental condition. This suggests that these two proteins may account for a very basic mechanism of interaction with siRNA-LNP. The third most upregulated protein differed between the four groups while haptoglobin (HP) was the fourth most strongly induced protein of all groups exhibiting a 7- to 14-fold statistically significant induction (Figure 2B). Additional liver proteins that were induced by the different conditions are shown in Figure S5 (Supporting Information).

A large number of proteins are generated by liver cells (hepatocytes) and therefore, it is important to identify proteins upregulated in the liver. Many proteins that are generated in the liver are also secreted into the circulation. We found that this liver-serum relation accounted in particular for HP which was the most upregulated serum protein exhibiting a 394- to 580-fold induction as apparent in the Volcano plot (Figure 2C). The second and third most enriched serum proteins were Serpin Family A Member 3N (SERPINA3N) and APOD (Figure 2D). While APOD can likely be linked to an interaction with APOE, the functional links of HP and SERPINA3N were not obvious. We therefore explored potential functional connections with other proteins using the software STRING,^[19] demonstrating that HP has links to APOE (Figure 2E), and that SERPINA3N was linked to HP (Figure 2F). Extended evaluations of serum proteins include VENN diagrams (Figure S6A, Supporting Information), enrichment analyses (Figure S6B, Supporting Information), heatmaps (Figure S7, Supporting Information), and graphs for supplementary key proteins (Figure S8, Supporting Information).

Since we found these clear links, i.e., of HP to apolipoproteins, we quantified the serum levels of different apolipoproteins and proteins functioning in lipid transport using targeted proteomics. Hierarchical clustering analysis demonstrated that all apolipoproteins were clustered in one branch and that these were either upregulated or unaffected compared to the untreated control (Figure 3A).

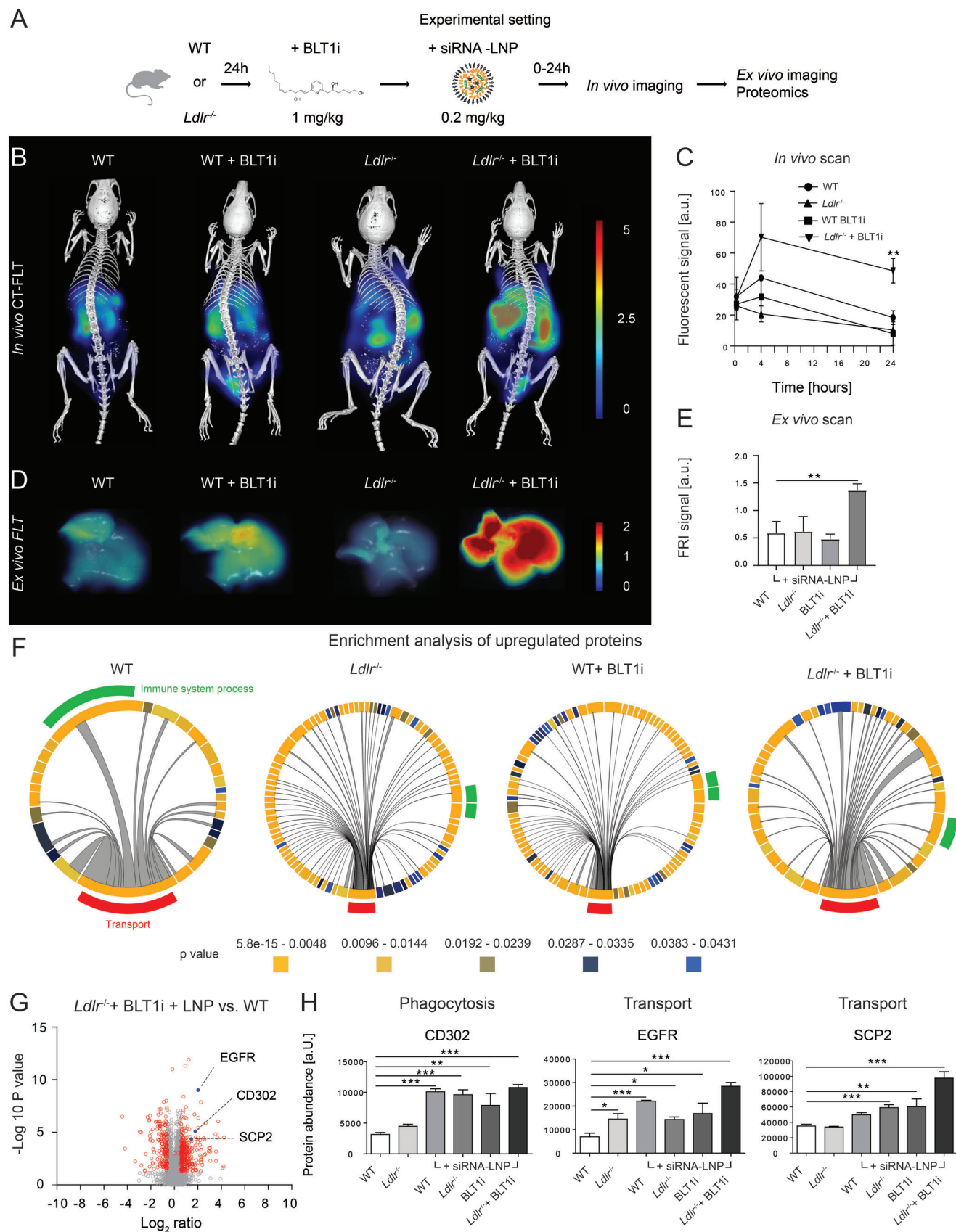


Table 2. Synopsis of significantly induced liver proteins and their biological functions.

All siRNA-LNP-groups	FC	Full name	Biological process
IFIT1	19.53	Interferon-induced protein with tetratricopeptide repeats 1	RNA binding
ISG15	13.25	Ubiquitin-like protein ISG15	RNA binding
IFIT3	4.17	Interferon-induced protein with tetratricopeptide repeats 3	RNA binding
HP	8.13	Haptoglobin	Transport
CMPK2	4.13	Cytidine/uridine monophosphate kinase 2	Nucleotide synthesis
STAT1	8.10	Signal transducer and activator of transcription 1	Immune system
OASL1	4.9	2"-5"-Oligoadenylate synthetase like	RNA binding
ORM1, AGP1	4.8	Orosomucoid-1, alpha-1-acid glycoprotein 1	Transport
TGTP2	4.8	T-cell-specific guanine nucleotide triphosphate-binding protein 2	Immune system
RNF213	4.6	E3 ubiquitin-protein ligase RNF213	Sensor protein
CD302, CLEC13A	3	CD302 antigen, C-type lectin domain family 13 member A	Phagocytosis
TM9SF4	2	Transmembrane 9 superfamily member 4	Phagocytosis
APOA4	2	Apolipoprotein A4	Transport
WT + siRNA-LNP			
MBL2	3	Mannose-binding protein C	RNA binding
CSRP1	2	Cysteine and glycine-rich protein 1	RNA binding
<i>Ldlr</i> ^{-/-} + siRNA-LNP			
NA	NA	NA	NA
BLT1i + siRNA-LNP			
H1-5	1.4	Histone H1.5	Monocyte histone
<i>Ldlr</i> ^{-/-} BLT1i + siRNA-LNP			
CYP2D9	18	Cytochrome P450 2D9	Lipid metabolism
ISYNA1	5	Inositol-3-phosphate synthase 1	Lipid metabolism
EGFR	4	Epidermal growth factor receptor	RM endocytosis
SCP2	3	Sterol carrier protein 2	Transport
MUP3	2	Major urinary protein 3	Transport
HBB-Y	1.8	Hemoglobin subunit epsilon-Y2	Transport
HDLBP	1.6	High density lipoprotein-binding protein	Transport
CMAH	1.6	Cytidine monophosphate-N-acetylneuraminic acid hydroxylase	Immune system
SLC16A1	1.5	Monocarboxylate transporter 1	Drug transport
SLC39A7	1.5	Zinc transporter SLC39A7	Drug transport
RABP4	1.5	Ras-related protein Rab-4B	Intracellular transport

Proteins and fold change (FC), full names, and biological process involved.

We allocated the significantly affected proteins into four different groups: the first included those generally induced by siRNA-LNP such as APOD, lipopolysaccharide-binding protein (LBP), and lecithin-cholesterin acyltransferase (LCAT). The second group included proteins significantly affected by *Ldlr*

deficiency such as APOB, APOE, and proprotein convertase subtilisin/kexin type 9 (PCSK9). The third group was composed of proteins of the BLT1i-*Ldlr*^{-/-} group such as APOC4, low-density lipoprotein receptor related protein 1 (LRP1, CD91), and C-reactive protein (CRP). APOC1, APOC3, and APOM

Figure 1. Inhibition of the immune cell specific Leukotriene B4 receptor evokes an accumulation of siRNA-LNP (lipid nanoparticles) in liver. A) Experimental setting. B) Noninvasive hybrid microcomputed fluorescence molecular tomography (CT-FLT) was done for 0.25, 4, and 24 h postinjection, here the 24-h time-point is shown. C) Quantifications of the in vivo imaging signals in liver. D) Fluorescence reflectance imaging (FRI) of the excised livers from panel B, and E) quantifications of the FRI signals. F) Enrichment analysis of proteins upregulated in each experimental group is reflected by the inner ring whereas the outer ring visualizes key groups only but is not related to significance. Key groups are highlighted in color. G) Volcano plot of the *Ldlr*^{-/-} + BLT1i group and H) selected key proteins identified. Data represent mean of $n = 2-5 \pm \text{SD}$; * $p < 0.05$, ** $p < 0.01$, *** $p < 0.001$ (One-way ANOVA).

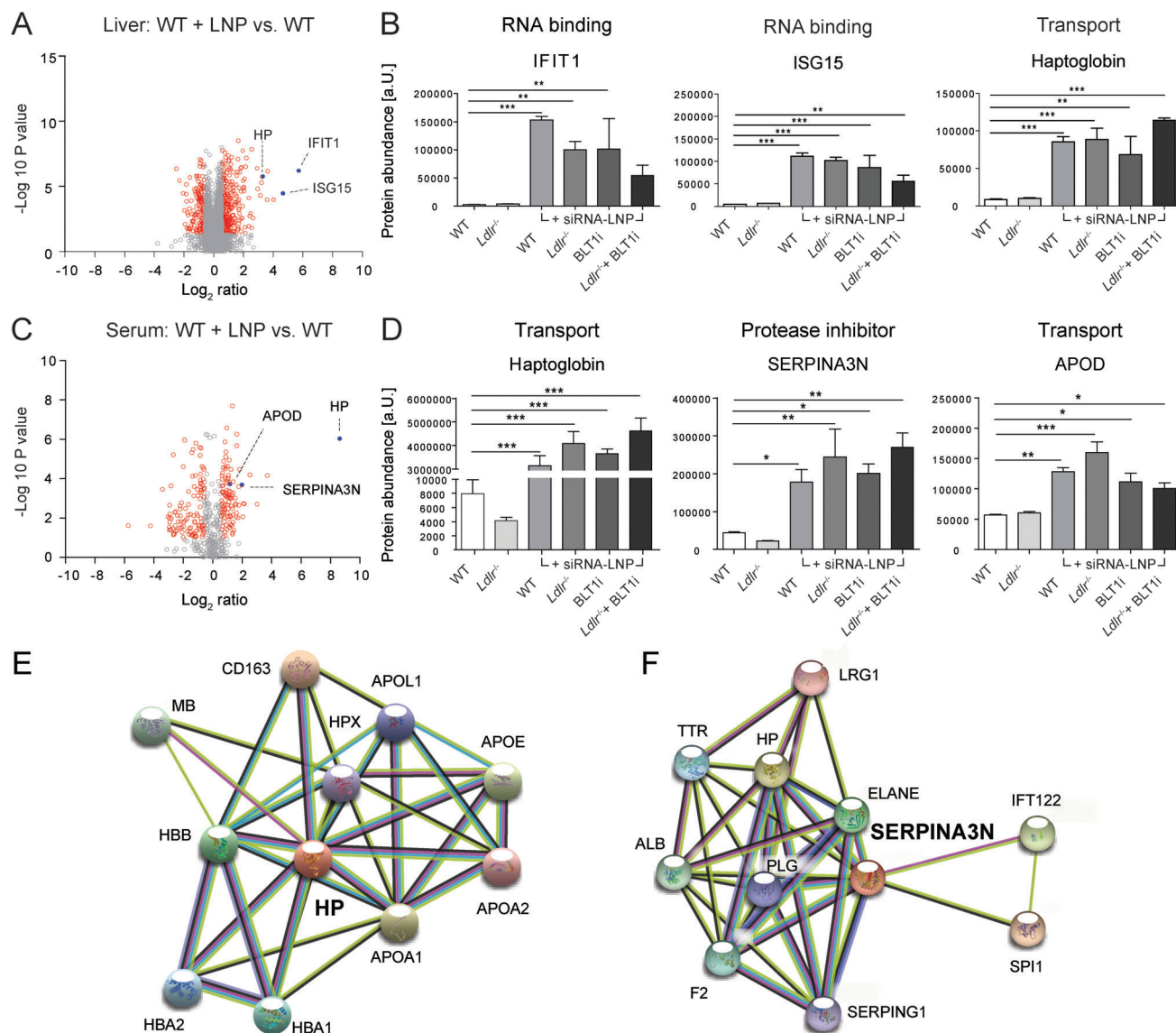


Figure 2. siRNA-LNP (lipid nanoparticles) induced proteins in liver and serum. Treatment as described in Figure 1A. A,C) Volcano plots showing A) key proteins induced by siRNA-LNP in wild-type (WT) mice, B) abundancies of selected proteins. C) Serum proteins upregulated upon siRNA-LNP injection. D) Selected serum proteins that were elevated upon administration of siRNA-LNP. E) Functional protein association of haptoglobin (HP) and F) SERPINA3N. Data represent mean of $n = 2-5 \pm SD$; * $p < 0.05$, ** $p < 0.01$, *** $p < 0.001$ (One-way ANOVA).

were significantly increased in the fourth group designated as BLT1i-*Ldlr*^{-/-} (Figure 3B). Except of APOA1, APOA2, and APOA4, all apolipoproteins were significantly affected by the siRNA-LNP (see Figure S9, Supporting Information, for the additional serum proteins). Synopses on the whole spectrum of elevated serum proteins from both untargeted and targeted proteomics including their regulation and significance are shown in Table 3.

These data demonstrate that specific changes in several apolipoproteins levels occur upon siRNA-LNP administration and these reflect specific treatment conditions. Genetic factors such as those of *Ldlr*^{-/-} mice have a major impact on the serum levels of apolipoproteins B and E whereas the amount of APOD was increased by the siRNA-LNP as such.

2.3. siRNA-LNP Lead to the Downregulation of Proteins Involved in Liver Detoxification and of Serum Opsonins

While the upregulated proteins were associated with transport functions and RNA binding, the data raised the question which proteins were reduced in liver and serum. We therefore visualized the 20 most downregulated proteins in the liver in a heatmap with clustering (Figure 4A). The Volcano plot of siRNA-LNP injected into WT mice demonstrated that proteins involved in liver detoxification such as the cytochrome P450 2A4 and 2A5 (CYP2A4 and CYP2A5) and sulfotransferase family 2A member 1 (SULT2A1) were the most significantly downregulated proteins in liver (Figure 4B). Quantifications of the abundances of these proteins further clarify their prominent reduction in the

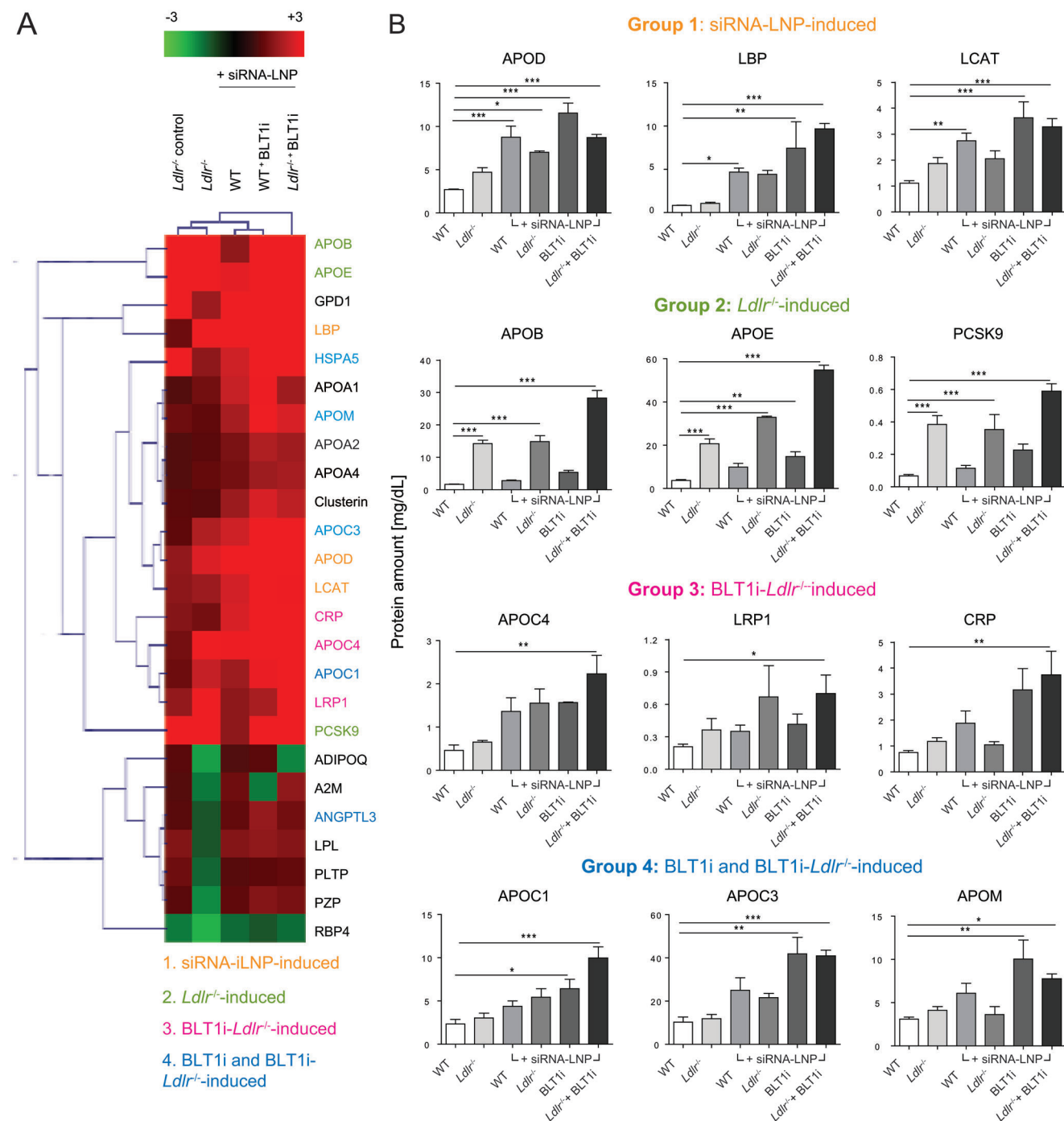


Figure 3. Quantification of serum apolipoproteins induced by siRNA-LNP (lipid nanoparticles). Treatment as described in Figure 1. A) Heatmap with hierarchical clustering analysis for conditions and proteins based on the fold change (FC) compared to serum of untreated wild-type (WT) mice. B) Quantifications of the protein content. Data represent mean of $n = 2-5$ independent experiments \pm SD; * $p < 0.05$, ** $p < 0.01$, *** $p < 0.001$ (One-way ANOVA).

liver, irrespective of treatment or genetic deficiency (Figure 4C). A synopsis on the regulation and significance of other liver proteins is provided with Table 4. Corroborating these findings in liver tissue, we noted a strong reduction of a serum protein involved in lipid metabolism, oxysterol binding protein like 3 (OSBPL3). In addition, we observed significant reductions

of immunoglobulin serum protein such as immunoglobulin kappa constant (IGKC) and Ig lambda-2 chain C region (IGLC2) (Figure 4D,E and Table 5).

These data show that the classical metabolic enzymes in liver and serum and levels of various opsonins (immunoglobulins) in serum were reduced by the siRNA-LNP.

Table 3. Synopsis of significantly induced serum proteins and their biological functions.

All siRNA-LNP-groups	FC	Full name	Biological process
HP	394-580	Haptoglobin	Transport
SERPINA3N	4-6	Serpin Family A Member 3	Protease inhibitor
APOD	3-4	Apolipoprotein D	Lipid transport
ITIH3	2-3	Inter-alpha-trypsin inhibitor heavy chain 3	RNA binding
WT + siRNA-LNP			
NA		NA	NA
Up in <i>Ldlr</i> ^{-/-}			
APOB	9	Apolipoprotein B	Transport
APOE	9	Apolipoprotein E	LNP binding
RUNDC3A	7	RUN domain-containing protein 3A	Cell proliferation
COL1A1	6	Collagen type I alpha 1 chain	Tissue remodeling
COL1A2	4	Collagen type I alpha 2 chain	Tissue remodeling
PM20D1	-2 to +7	N-fatty-acyl-amino acid synthase/hydrolase PM20D1	Proteolysis
BLT1i + siRNA-LNP			
APOM	3	Apolipoprotein M	Lipid transport
LCAT	2-3	Phosphatidylcholine-sterol acyltransferase	Lipid transport
APOC3	2	Apolipoprotein C3	Lipid transport
<i>Ldlr</i> ^{-/-} BLT1i + siRNA-LNP			
SERPINA1E	5-31	Serpin A1E	Protease inhibitor
LBP	5-12	Lipopolysaccharide-binding protein	Lipid transport
APCS	6-11	Serpin peptidase inhibitor, Clade A, Member 1	LDL particle binding
APOC4	3-5	Apolipoprotein C4	Lipid transport
APOC1	2-4	Apolipoprotein C1	Lipid transport
LRP1	2-3	LDL Receptor Related Protein 1	LDLR-related
CRP	2-5	C-Reactive protein	Immune response

Proteins and fold change (FC), full names, and biological process involved.

2.4. Inhibition of the HDLR Leads to Reduced Hepatic Uptake of siRNA-LNP and a Predominant Accumulation in Myeloid Immune Cells in the Circulation and the Liver

We observed that targeting a small molecule-based inhibitor of immune cell infiltration and activation leads to increased hepatic uptake of siRNA-LNP. Importantly, this added a lot to our understanding of transport processes induced by the presence of these particles. It suggests that there is a competition between the liver and the immune cells for siRNA-LNP biodistribution. Therefore, the next aim was to verify if we could achieve the opposite effect by inhibiting a key receptor for hepatic uptake of lipids. We therefore adapted the experimental setting from the previous experiments by replacing the LTB4 inhibitor with a second small molecule that works as inhibitor for the HDLR (HDLRi). Here, we used a commercial negative control siRNA labeled with an Alexa fluor 647 label to generate siRNA-LNP that is detectable in ex vivo FRI scans and multicolor flow cytometry. The dosage of 0.6 mg kg⁻¹ body weight allowed for an optimal visualization of siRNA uptake in FRI. We analyzed the mice 24 h after the injection of the siRNA-LNP using FRI-based ex vivo imaging (Figure 5A). It could be shown that the HDLRi strongly reduced liver uptake, but evoked increased uptake in the spleen.

The HDLRi-*Ldlr*^{-/-} mice and, to a lower extent, the *Ldlr*^{-/-} mice exhibited a higher uptake in the spleen compared to the liver (Figure 5B).

The next aim was to study the uptake of the siRNA-LNP by immune cells in the circulation and the liver using flow cytometry. We observed that the HDLRi or *Ldlr*^{-/-} only had slight, but no statistically significant effects on the immune cell frequencies in the liver (Figure 5C, Figure S10, Supporting Information). Strikingly, the HDLRi significantly increased the number of circulating neutrophils by a factor of 20 and induced monocytes fivefold. The monocyte elevation mostly affected the inflammatory Ly6C^{high} monocyte subpopulation. On the contrary, the cell count of blood lymphocytes (CD19⁺/CD3⁺) was unaffected (Figure 5D, Figure S11, Supporting Information). Despite the comparatively low signal observed in the FRI scan of the livers (Figure 5B), the uptake of siRNA-LNP by liver leukocytes increased significantly upon HDLRi treatment, led to a 150-fold induction in hepatic dendritic cells (Figure 5E) and evoked a 50-fold induction in monocyte-derived macrophages (Figure S12B, Supporting Information). The HDLRi also led to an increased uptake by B cells, but the induction was as little as threefold, while the uptake induction for T cells was twofold, and there was no elevation by NK cells (Figure S12C, Supporting Information). The

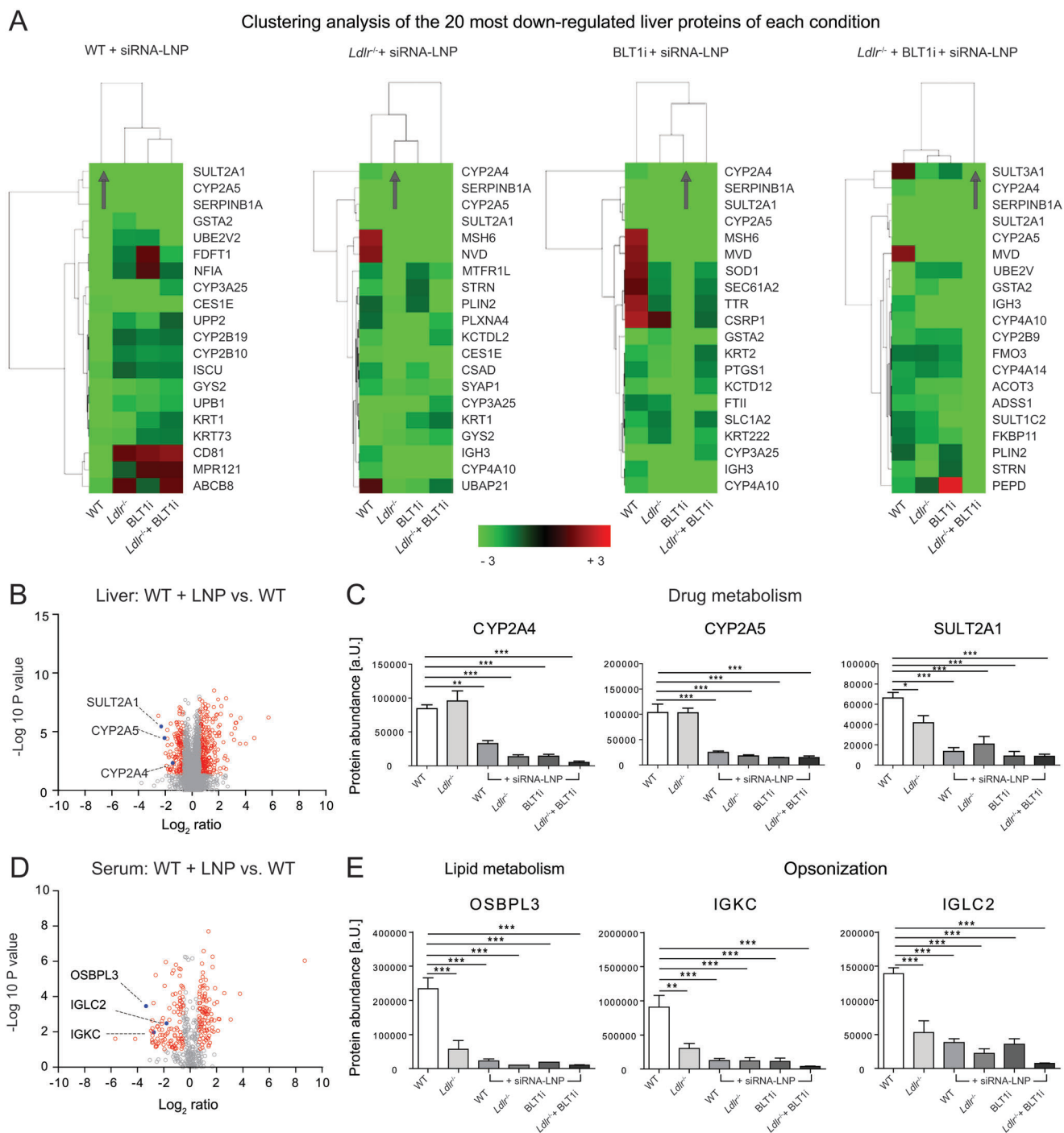


Figure 4. Downregulation of proteins involved in liver detoxification and of serum opsonins upon siRNA-LNP (lipid nanoparticles) injection. Treatment as in Figure 1A. A) Heatmaps with HCA of the 20 most downregulated proteins as identified in untargeted proteomics normalized to tissue of untreated wild-type (WT) mice. B) Volcano plot with key proteins lowered by siRNA-LNP highlighted. C) Relative protein abundances of selected key downregulated proteins. D) Volcano plot from untargeted serum proteomics with serum proteins highlighted that decreased upon siRNA-LNP administration. E) Relative protein abundances of selected key downregulated proteins. Data represent mean of $n = 2-5 \pm \text{SD}$; * $p < 0.05$, ** $p < 0.01$, *** $p < 0.001$ (One-way ANOVA).

Table 4. Synopsis of significantly reduced liver proteins and their biological functions.

All siRNA-LNP-groups	FC	Full name	Biological process
CYP2A4	−18	Cytochrome P450 2A4	Drug metabolism
SULT2A1	−8	Sulfotransferase 2A1	Drug metabolism
CYP2A5	−7	Cytochrome P450 2A5	Drug metabolism
CD36	−2		Fatty acid transport
WT + siRNA-LNP			
MRPL21	−3	39S ribosomal protein L21, mitochondrial	RNA binding
CYP2B19	−3	Cytochrome P450 2B19	Particle-regulated
<i>Ldlr</i> ^{−/−} + siRNA-LNP			
NA	NA	NA	NA
BLT1i + siRNA-LNP			
THRAP3	−2 to +3	Thyroid hormone receptor-associated protein 3	RNA processing
<i>Ldlr</i> ^{−/−} + BLT1i + siRNA-LNP			
FMO3	−4	Dimethylaniline monooxygenase [N-oxide-forming] 3	Lipid metabolism

Proteins and fold change (FC), full names, and biological process involved.

Table 5. Synopsis of significantly reduced serum proteins and their biological functions.

All siRNA-LNP-groups	FC	Full name	Biological process
OSBPL3	−24 to −11	Oxysterol binding protein like 3	Lipid metabolism
IGLC3	−5 to −29	Immunoglobulin lambda constant 3	Opsonization
IGKC	−7 to −24	Immunoglobulin kappa constant	Opsonization
GM5571 (IGKV9-120)	−5 to −22	Immunoglobulin kappa chain variable 9–120	Opsonization
IGLC2	−3 to −19	Immunoglobulin lambda constant 2	Opsonization
IGHV3-6	−7 to −16	Ig heavy chain V region 3–6	Opsonization
IGH3, IGHG2B	−4 to −16	Immunoglobulin heavy constant gamma 2B	Opsonization
WT + siRNA-LNP			
NA	NA	NA	NA
<i>Ldlr</i> ^{−/−} + siRNA-LNP			
NA	NA	NA	NA
BLT1i + siRNA-LNP			
PF4, CXCL4	−5	Platelet factor 4, C–X–C motif chemokine 4	Immune response
<i>Ldlr</i> ^{−/−} + BLT1i + siRNA-LNP			
A1BG	−3 to 78	Alpha-1-B glycoprotein	Immune response

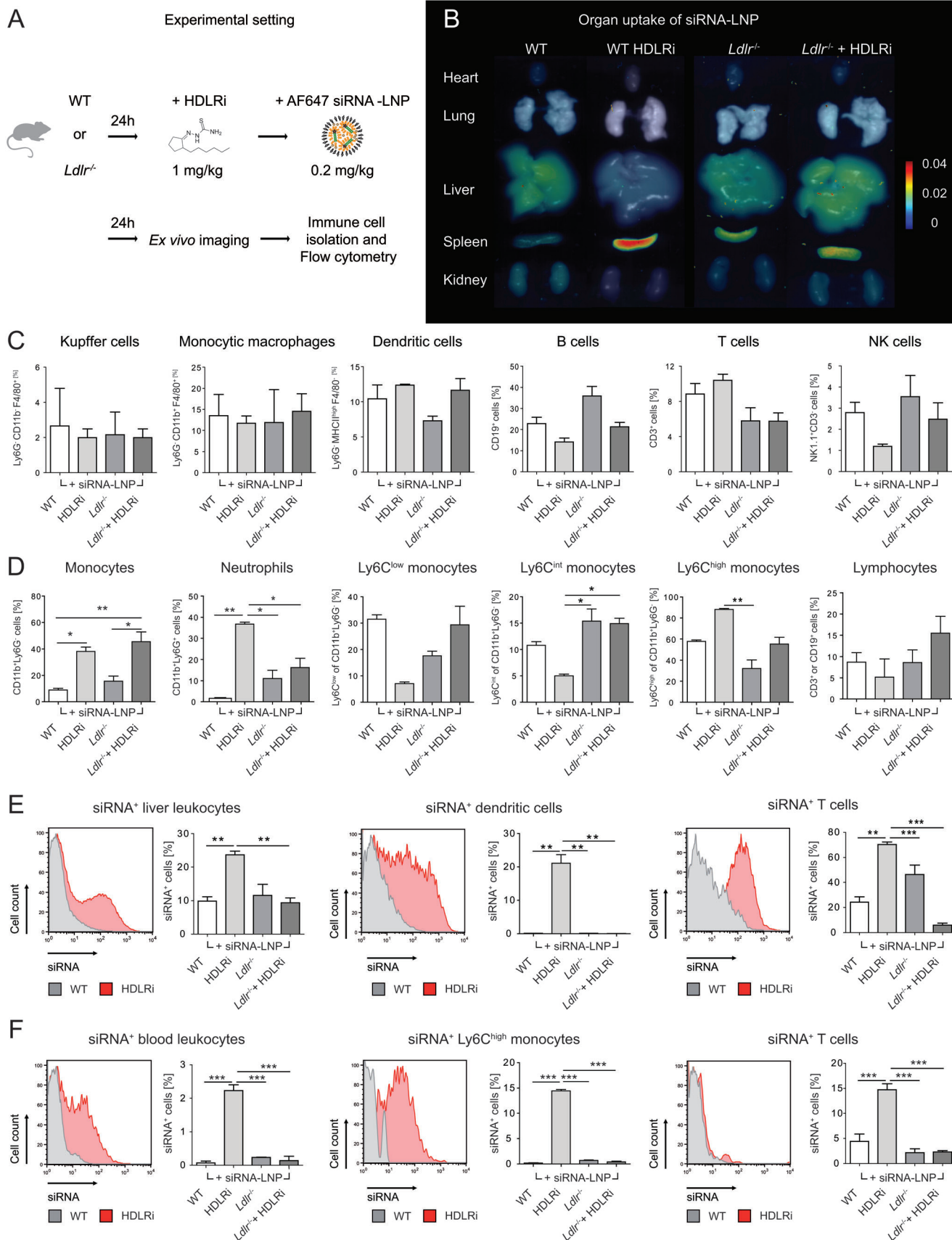
Proteins and fold change (FC), full names, and biological process involved.

accumulation of siRNA-LNP in blood leukocytes was generally much lower than by hepatic leukocytes (about 10 times less). The particles mostly accumulated in neutrophils and monocytes (Figure S13A–C, Supporting Information) and were enriched in the Ly6C^{high} subset. The uptake of siRNA-LNP by blood B, T, and NK cells was very low (Figure 5F, Figure S13D, Supporting Information).

In summary, these data demonstrate that the HDLri leads to a significant reduction of the hepatic uptake of siRNA-LNP and induces an enrichment of LNP-formulated siRNA in myeloid immune cells in the circulation and the liver.

2.5. HDLri Inhibition Leads to Upregulation of Factors for Leukocyte Recruitment and for Transcripts Functioning in Transport Processes

The HDLri apparently has the potential to be used for enhancing the uptake of siRNA-LNP into myeloid cells. This might allow targeted delivery of siRNA and other types of small noncoding RNA into liver immune cells using LNP. Seeking to comprehend our understanding of the actions of the HDLri on liver tissue and to search for potential off-target effects, we performed RNA sequencing of liver tissue. Compared to proteomics, RNA



seq can identify about four times more transcripts than proteins. The limitation of the proteomics technique is that it does not provide full coverage of receptors and cytokines. We thus compared 0.2 mg kg⁻¹ of siRNA-LNP to a pretreatment with the HDLRI and subsequent treatment with the same amount of siRNA-LNP in a new experiment. Enrichment analysis of transcripts revealed that the HDLRI-induced transcripts act on the plasma membrane and cellular periphery whereas the siRNA-LNP without the inhibitor led to the enrichment of transcripts involved in extracellular processes. Both experimental groups were enriched with transcripts functioning intracellularly (Figure 6A).

The siRNA-LNP (with and without HDLRI) led to strongly enhanced expression of the C–X–C Motif Chemokine Ligand 9 (Cxcl9) that functions in leukocyte recruitment, and also to increased expression of Cd200 in the tissue, a receptor that has immunoregulatory function. We detected two transcripts that were regulated by the siRNA-LNP, but not by the additional inhibitor: Isg15, an RNA binding protein, was increased, and the scavenger receptor Cd163 expressed by hepatic macrophages was downregulated by the particles (Figure 6B). The HDLRI combined with the particles, but not the particles alone led to a significantly increased transcript abundance of C–X–C Motif Chemokine Ligand 1 (Cxcl1), the Serine proteinase inhibitor, clade A, member 3C (Serpina3c), as well as serum amyloid A 1 (Saa1) and Saa2 (Figure 6C). An overview on the transcripts that were affected by the siRNA-LNP and the HDLRI is given in Table 6.

Interestingly, four transcripts that reflect hepatotoxicity,^[20] carnitine O-acetyltransferase 3 (Crat), carbonic anhydrase 3 (Car3), cytochrome P450 family 39 subfamily A member 1 (Cyp39a1), and solute carrier family 39 member 1 (Slc39a1) were unaffected. Furthermore, the four apolipoprotein transcripts that could be detected (ApoE, Apoh, Apob, and ApoA4), were all not differentially regulated. In addition, no other receptor that might be responsible for siRNA-LNP uptake except for Cd163 was significantly affected on transcript level. In detail, we have studied the transcript abundances of the Ldlr, very-low density lipoprotein receptor (Vldlr), Hdlr (Scarb1), cluster of differentiation 36 (Cd36) that is also known as platelet glycoprotein 4, fatty acid translocase (Fat), those of the Egfr, macrophage scavenger receptor 1 (Msr1), Stabilin 1 (Stab1), and macrophage receptor with collagenous structure (Marco), which were all unaffected. Also, Saa-response transcripts (Fpr2 and Abca1) and inflammatory factors (Ltb4r1 and Il1 β) were unaffected (Figure S14, Supporting Information).

In line with the findings of the flow cytometry, the RNA sequencing data identified an induction of Cxcl1 and Cxcl9 chemokines in liver tissue, both of which are known to attract specific leukocytes into the liver. The gene expression data further indicate that Saa1 and Saa2 upregulation may relate to transport processes, but rather do not reflect an acute phase response in which Saa1 and Saa2 are also involved. The expected role for transport processes, but not inflammatory processes is also suggested because the key inflammatory indicator Il1 β was not regulated.

3. Discussion and Conclusions

We consider the lipid formulation that is used in the first siRNA-based drug Onpattro^[2] as an important benchmark in the field. While many groups aim at optimizing the compositions of the LNP for the targeting of specific organs or cells, our approach was to use small molecule-based inhibitors to manipulate the cellular distribution of siRNA-LNP to gain mechanistic understanding of siRNA-LNP biodistribution. This has the advantage that the approved formulation of Onpattro (of which all components are commercially available) can be used to manipulate the biodistribution of siRNA-LNP.

The acceleration of the hepatic uptake into *Ldlr*^{-/-} mice upon inhibition of the LTB4 receptor suggests that the immune cell compartment plays an unprecedented role for hepatic clearance of siRNA-LNP. The increased hepatic intake can be led back to the lower numbers of myeloid immune cells such as neutrophils, macrophages, and dendritic cells in the liver.^[21] The inhibitor may thus increase the availability of siRNA-LNP for hepatocytes because the presence of immune cells is reduced. This enhanced uptake was particularly remarkable because the *Ldlr*^{-/-} mice are actually known to internalize less LNP into the liver compared to WT animals.^[3] The increased hepatic intake was accompanied by the induction of distinct proteins that play a role in phagocytosis and transport processes. The receptor CD302 exhibited the highest levels in the *Ldlr*^{-/-} and BLT1 group, which is potentially an interesting observation because this receptor is involved in endocytosis and phagocytosis,^[22] and may therefore be involved in the uptake of siRNA-LNP into the liver. A similar expression pattern as for CD302 was found for the epidermal growth factor receptor (EGFR) that is expressed by hepatocytes.^[5]

The HDLRI strikingly led to the opposite effect as the LTB4 receptor: it reduced the hepatic intake and directed the LNP into myeloid immune cells. It is certain that the high levels of Cxcl1 induced by the HDLRI are the reason for neutrophil recruitment.^[23] The reason for the pronounced, but insignificant elevation of Cxcl9 mRNA both by siRNA-LNP with or without the HDLRI remains elusive since the chemokine ligand CXCL9 is expressed by hepatocytes, hepatic stellate cells, and liver endothelial cells whereas the receptor for CXCL9, CXCR3, is expressed by KC, hepatic stellate cells, and liver endothelial cells.^[24] It is also known that Cxcl9 leads to enhanced T-cell recruitment in liver disease.^[25] Until now, there is thus no clear explanation for the induction of Cxcl9 by the LNP and the HDLRI.

Recently, various other attempts aimed to increase RNA delivery to myeloid immune cells with LNP: specific lipids were incorporated into the lipid mixture of LNP,^[26] LNP-coupled antibodies directed against myeloid cells were used,^[14,15] mannoseylated LNP were generated that target myeloid cells based on their mannose receptor,^[13] and anionic RNA-LNP were generated.^[17] To our knowledge, the 50- to 150-fold increase in hepatic myeloid cell targeting that we found in vivo is the most profound acceleration in myeloid targeting by LNP observed so far. It for example by far

Figure 5. Effects of high-density lipoprotein receptor inhibitor (HDLRI) inhibition on the uptake of siRNA-LNP (lipid nanoparticles) by immune cells in liver and blood. A) Experimental setting. B) Fluorescence reflectance imaging of selected organs. C) Counts of immune cells count in liver and D) blood. E) Distribution of siRNA-LNP in different leukocytes in liver and F) blood. Data represent mean \pm SD of $n = 2$; * $p < 0.05$, ** $p < 0.01$, *** $p < 0.001$ (One-way ANOVA).

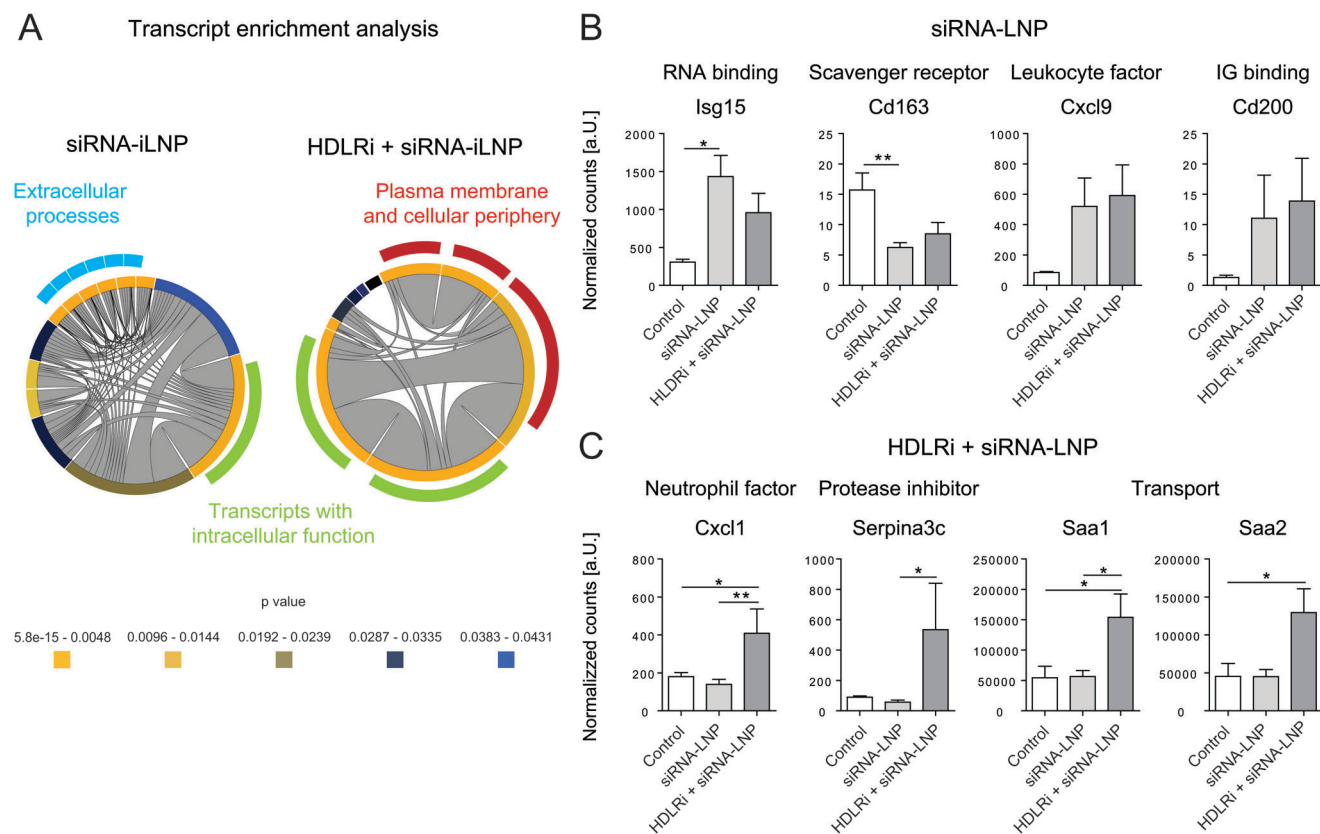


Figure 6. Effects of siRNA-LNP (lipid nanoparticles) and high-density lipoprotein receptor inhibitor (HDLRi) inhibition on hepatic gene expression. C57BL/6J mice received siRNA-LNP at 0.2 mg kg⁻¹ and the other group was pretreated with the HDLRi for 24 h prior to siRNA-LNP injection. RNA sequencing of liver tissue was done. A) Enrichment of groups of RNA transcripts induced upon treatment with siRNA-LNP or HDLRi + siRNA-LNP. The *p* value scale applies to the inner ring only whereas the outer ring was added to visualize key protein groups only but is not related to significance. B) Regulations of transcripts by siRNA, that were enriched in the siRNA-LNP group. C) Transcripts induced by HDLRi + siRNA-LNP. Data represent mean \pm SD of *n* = 4–6; **p* < 0.05, ***p* < 0.01, ****p* < 0.001 (One-way ANOVA).

Table 6. Synopsis of significantly regulated hepatic gene expression and biological processes.

By siRNA-LNP	FC	Full name	Biological process
Ifit3	5	Interferon-induced protein with tetratricopeptide repeats 3	RNA binding
Isg15	3-4	Ubiquitin-like protein ISG15	RNA binding
Ifit1	3	Interferon-induced protein with tetratricopeptide repeats 1	RNA binding
Cd163	2	Hemoglobin scavenger receptor	Scavenger receptor
By HDLRi + siRNA-LNP			
Serpina3c	9	Serine protease inhibitor A3C	Protease inhibitor
Saa1	3	Serum amyloid A-1	Transport
Saa2	2	Serum amyloid A-2	Transport
Cyp2a5	2	Cytochrome P450 2A5	Lipid metabolism
Cxc1	2	C-X-C motif chemokine 1	Neutrophil recruitment
Igk2	–3	Immunoglobulin lambda constant 2	Opsonization

Gene expression fold change (FC), full names, and biological process involved.

exceeds the effects of mannosylated nanoparticles that reported a fourfold increased targeting of hepatic macrophages.^[27] The enhanced uptake of the siRNA by the Ly6C^{high} monocytes upon HDLri pretreatment indicates that Ly6C^{high} monocytes transport the siRNA from the circulation into the liver where this subset of monocytes differentiates into MoMF and DC.^[28] In contrast, the HDLri-mediated uptake acceleration by KC that originate from the liver was much lower than by the MoMF and DC that continuously are replenished in the liver by monocytes. This is in line with earlier studies of our group using gold nanoparticles, which were mostly located in the monocytic macrophages, and to a significantly lower extent inside the KC.^[11a] Taken together, the two different small molecules apparently act on critical points of LNP biodistribution and thereby enable shifting the balance of siRNA-LNP accumulation to either liver or immune cells, respectively.

Recent research pointed out in a large screening of LNP formulations that interactions of RNA-LNP apart from APOE affect their tendency of enrichment in different cell types.^[29] In line with this, our proteome data indicate that the levels of APOE as such cannot explain differences in the uptake that we observed between the different experimental conditions. We therefore assume that other proteins, particularly those in serum such as HP or SAA, that are functionally linked to APOE have an indirect but more important impact on the transport processes of RNA-LNP. It is very likely that HP plays a key role, because it is both a ligand of APOE^[30] and a component of HDL particles.^[31]

While the role of HP for LNP transport remains to be studied in more detail, the transportation function for LNP by association with APOA1, APOC2, APOD, and APOE was demonstrated before.^[32] It is of course not surprising that RNA-binding proteins were induced by siRNA-LNP. It was stated that 2961 genes encode for such proteins in humans.^[33] Particularly IFIT1 and ISG15 have been reported to have an RNA-binding function before.^[34] Thus, it appears very likely that these RNA-binding proteins were induced by the siRNA-LNP. The hepatic induction of Saa1 and Saa2 suggests that these two proteins, which can function as apolipoproteins,^[35] contribute to the specific immune-cell tropism of the siRNA-LNP that occurs upon treatment with the HDLri. Moreover, SAA is lipidated by hepatocytes, what suggests that SAA may function by binding to the siRNA-LNP, and may thereby affect transport processes. Furthermore, the plasma clearance of SAA occurs more rapid than that of the other major HDL apolipoproteins, ApoA1 and ApoA2.^[35] This suggests a role of SAA1 and SAA2 in the transport of siRNA-LNP.

The reduction of proteins functioning in drug and lipid metabolism in the liver and serum suggests that they mediate the degradation of the siRNA-LNP since it is known that CYP2A4 and CYP2A5 are associated with lipid metabolism.^[36] The SULT proteins function in the sulfonation of various molecules what generally increases their water solubility and reduces their toxicity.^[37] Thus, SULT2A1 might be involved in degrading parts of the LNP lipid fraction and their consumption in biochemical reactions may explain their deprivation in the liver and serum.

The reduction of serum opsonins (IGLC3, IGKC, GM5571, IGLC2, and IGHV3-6) might be owed to their unspecific binding to the siRNA-LNP. Particularly, IGLC2 is present at the protein corona of PEGylated LNP.^[38] Comparable findings exist for IGLC3,^[39] and IGKC.^[40] Immunoglobulins are abundant serum proteins and it has for instance been shown that IGKC belongs

to the 25 most abundant serum proteins.^[40] We thus hypothesize that these proteins indeed bind to the siRNA-LNP and impact their clearance.

We are aware that our study has limitations. One limitation lies in the fact that the molecular analyses cover only the 24-h time point, what cannot reflect the actual dynamics of gene and protein expression. Nevertheless, the big data generated unraveled a huge number of potential novel players in the field and current experiments of our lab aim to clarify the role of the various proteins identified. Furthermore, each imaging technique has its limitations. The incorporation of a Cyanine 7 dye with a carboxylic chain might be criticized as being unstably entrapped into the siRNA-LNP. Importantly, we have demonstrated that the size and surface charge of the siRNA were not affected by the incorporated dye, indicating that the particles were very comparable to those without dye or with a labeled siRNA.

In this study, we have intensively studied the role of immune cells for the hepatic uptake of siRNA-LNP. We conclude that the balance in the biodistribution of siRNA-LNP between immune cells and liver parenchymal cells can be modified with small molecules. These findings are of potential interest for applications of RNA delivery to hepatic or extrahepatic targets.

4. Experimental Section

siRNA and Lipids: Positive control Dsi-RNA against Hprt1 mRNA was purchased from IDT (Coralville, IA, USA). Alexa Fluor 647-labeled negative control siRNA was purchased from Qiagen (AllStars siRNA). The ionizable lipid heptatriaconta-6,9,28,31-tetraen-19-yl-4 (dimethylamino) butanoate (MC3) was obtained from Hycultec GmbH (Beutelsbach, Germany). The helper lipid 1,2-distearoyl-sn-glycero-3-phosphorylcholine (distearoyl-phosphatidylcholine) (DSPC), and the polyethylene (PEG) lipid 1,2-dimyristoyl-rac-glycero-3-methoxypolyethylene glycol-2000 (DMG-PEG 2000), and cholesterol were purchased from Sigma-Aldrich (St Louis, MO).

Generation and Characterization of siRNA-LNP: The siRNA-LNP used in this study were prepared using a NanoAssemblr Spark (Precision Nanosystems Inc., Vancouver, Canada). The lipid components (MC3, DSPC, Chol, and PEG2000-lipid) were dissolved in absolute ethanol and mixed at a molar ratio of (50:10:38.5:1.5) to achieve a total concentration of 50×10^{-3} M of lipid mix. The aqueous phase was prepared by dissolving the RNA in sterile 0.1 M acetate buffer. The LNP were formulated according to the instructions of the manufacturer using setting 3. LNP were stored at 4 °C until usage and used within 2 days. In order to enable molecular imaging of LNP, Cyanine 7 (Cy7) carboxylic acid (Lumiprobe, Hannover, Germany) was used by adding 1 mol% to the lipid mix.

Encapsulation efficiency (EE) of RNA into RNA-LNP was determined using a Quant-iT RiboGreen assay according to manufacturers' instructions (Thermo Fisher Scientific, Waltham, MA, USA). Briefly, samples were diluted 10-fold in tris(hydroxymethyl)aminomethan (TRIS) ethylenediaminetetraacetic acid (EDTA) (TE) buffer and incubated for 15 min at 37 °C in 1% (v/v) Triton X-100 (Sigma-Aldrich), to extract the encapsulated RNA. Samples were analyzed for fluorescence quantification on a microplate reader (Cytation 3, BioTek Instruments Inc., Winooski, VT, USA) at an excitation of 485 nm and an emission at 528 nm. EE in percent was determined as the difference between the total RNA and the non-encapsulated RNA, divided by the total RNA. Dosing of RNA-LNP was based on the EE.

Mice and Inhibitors: C57Bl/6J WT mice were obtained from Janvier (France) and B6-(Ldlr)tm were generated as described before.^[41] Animals were housed under specific pathogen free conditions at the animal facility of the University Hospital Aachen, as approved by the LANUV NRW under the animal grant number 81-02.04.2020.A302. The experiments were done in accordance with the EU Directive 2010/63/EU for animal exper-

iments and the ARRIVE guidelines (<https://arriveguidelines.org/arrive-guidelines>). Animal group sizes were not increased upon reaching significance compared to the respective control group. The Leukotriene B4 receptor inhibitor BLT1i was dissolved in ethanol, diluted with PBS, and administered at the dosage of 1 mg kg⁻¹ body weight via intravenous injection at a volume of 125 µL. The HDLRI (termed BLT-1) was diluted in DMSO used at the dosage of 1 mg kg⁻¹ body weight via intravenous injection at a volume of 20 µL, based on previous studies.^[42]

Imaging of siRNA-LNP Biodistribution: Mice received a chlorophyll free feed (Ssniff, low fat control diet[®] Cat-Nr. E15051) 1 week prior to the experiment, to reduce the background fluorescence signal. Anesthesia was initiated by 5% isoflurane (Forene, Abbott, Wiesbaden, Germany) in air enriched with oxygen using a vaporizer. Throughout the imaging process, the concentration of isoflurane was set to 2%. Mice were shaved under anesthesia on the day of experiment. Eye desiccation was prevailed using eye ointment (Bayer Vital GmbH, Germany). Intravenous injection into the lateral tail vein was made by a sterile catheter that was prepared through linking a 30 G cannula (B. Braun, Melsungen, Germany) with a polyethylene tube (the inner was 0.28 mm and the outer diameter was 0.61 mm, and the thickness of the wall was 0.165 mm) (Hartenstein, Würzburg, Germany). Mice were randomly assigned into the groups and were intravenously injected with siRNA-LNP dissolved in PBS at a volume of 125 µL.

The in vivo biodistribution of Cy7-labeled siRNA-LNP was assessed by a hybrid microcomputed tomography-fluorescence tomography (µCT-FLT) device (U-CT OI, MILabs B.V., Utrecht, the Netherlands). Anesthetized mice were positioned between two acrylic glass plates in the animal container, and placed flanked by the FLT laser and the CCD camera. About 130 points were acquired during the scan by a laser and filter with an excitation of 730 and an emission of 775 nm. After acquiring the FLT scan, the animal container was moved automatically to the CT for a total body scan that enables visualization of anatomical structures. During full rotations in a step-and-shoot mode, 480 projections (1944 × 1536 pixels) were attained with an X-ray tube voltage of 55 kV, a power of 0.17 mA, and an exposure time of 75 ms. This process was done for every animal prior to siRNA-LNP injection as well as 0.25, 4, and 24 h after the injection, in order to longitudinally visualize the fluorescence signal in different organs.

The animals were sacrificed using 10% isoflurane after the last µCT-FLT scan. Blood was collected, livers were perfused with PBS, and organs were excised for ex vivo evaluation. Images were acquired using a fluorescence molecular tomography device (FMT 400, PerkinElmer, Waltham, MA, USA) in 2D reflectance imaging mode at 750 nm excitation wavelength.

Flow Cytometric Analysis of Immune Cells: Blood coagulation was prevented prefilling insulin syringes with 50 µL of 0.5 M EDTA before taking blood. Cells were then subjected to erythrocyte removal by Pharm Lyse buffer (BD Bioscience). Single cells suspensions from liver tissue were generated by mincing the whole liver of each animal into pieces <1 mm using squissors and digestion with 2% collagenase IV (Worthington) for 30 min. In order to analyze the uptake of the fluorescently labeled siRNA by different immune cells based on the fluorescent signal of Alexa 647 dye, the cell pellets were suspended in 100 µL staining cocktail which consisted of 80 µL PBS, 20 µL of blocking buffer (serum mixture from 2% mouse, 2% rat, and 2% bovine serum albumin), and fluorochrome-conjugated antibodies to multicolor panels with CD45, CD11b, F4/80, CD4, CD8, CD19, MHCII, NK1.1, and Ly6G (all Miltenyi Biotec, Bergisch Gladbach).

The channel for APC color was used to quantify the Alexa fluor 647 signals of the siRNA-LNP. Cells were incubated for 30 min at room temperature and shielded from light at 4 °C. Subsequently cells were rinsed with 500 µL PBS to remove unbound antibodies upon centrifugation at 400 rcf rpm for 10 min, discarding the supernatant, and resuspension in 150 µL PBS. The single cell suspensions were recorded using a FACS Canto II flow cytometer (BD Bioscience) and analyzed by FlowJo 8.8.6 software as published earlier.^[11a] The quantification of leukocyte subtypes was done by designating CD45⁺ blood leukocytes with subgating neutrophils as CD11b⁺LyG⁺, monocytes as CD11b⁺LyG⁻, and discrimination of monocyte subsets was made based on their expression of Ly6C (gating Ly6G⁻ and Gr1⁺ defined as Ly6C), B cells as CD19⁺, lymphocytes as CD4⁺CD8⁺, and NK cells as CD4⁻ NK1.1⁺. In liver, lymphocytes were gated identical to blood cells and monocyte-

derived macrophages were defined as CD45⁺Ly6⁻CD11b⁺F4/80⁺, KC as CD45⁺Ly6⁻CD11b⁺F4/80⁻, dendritic cells as CD45⁺Ly6⁻MHCII⁺F4/80⁻, and neutrophils as CD45⁺Ly6⁺CD11b⁺F4/80⁺.

Proteomics Sample Preparation: Whole liver protein (from perfused liver) was generated from liver pieces sizing about 5 mm² using a Retch Mill using metal beads for tissue disruption, and RIPA buffer, as published before in detail.^[11a] In-gel digestion was performed on 50 µg total protein liver lysate sample or 1 µL serum sample as described previously.^[43]

Discovery-Based Proteomics: Discovery-based mass spectrometry was done using a quadrupole orbitrap mass spectrometer equipped with a nanoelectrospray ion source (Orbitrap Exploris 480, Thermo Scientific). Chromatographic separation of the peptides was exerted as described previously^[44] with the following adjustments: the flowrate was changed to 300 nL min⁻¹ and the gradient was set from 2% to 45% buffer B. Measurements were done with digests from an equivalent of 1 µg total protein starting material from the liver lysates or 50 nL digested serum. The mass spectrometer was used in the positive ion mode and data-independent acquisition (DIA) mode using an isolation windows of 12 m/z with a precursor mass range of 300–1200. LC–MS raw data were processed with Spectronaut (version 15.6.211220.50606, Biognosys) using the standard settings of the directDIA workflow, with a mouse SwissProt database (www.uniprot.org, 17 021 entries). For the quantification, local normalization was applied and the Q-value filtering was adjusted to the classical setting without imputing. For proteome data see DATA AVAILABILITY.

Targeted Proteomics: Selected reaction monitoring (SRM) analyses were performed as described previously,^[45] but with a protein panel against proteins related to the lipid metabolism. The following changes have been implemented: sample injection was done with digests from an equivalent of 50 nL starting material serum plus 1/0.1 ng isotopically labeled standard peptides (for the high/low abundant subset of targets in the panels, respectively) and the retention time scheduling windows were extended to 8 min for all peptides. The peptides that were used to target these proteins are shown in Table S1 (Supporting Information).

Bioinformatics Evaluation of Proteome Data: The output from discovery-based proteomics was used to calculate the protein expression fold change (FC) by dividing the mean amounts of every group by WT liver tissue. Using a cutoff of 1.5, this work defined groups of up or downregulated proteins from every experimental condition. These groups were subjected to protein enrichment analysis using the free online tool MonaGO.^[46] The setting in MonaGO was set to “Biological process” and the circular visualizations were modified to simplify data interpretation. Thus, only the inner ring from the graphical output of MonaGO was kept. The outer ring was manually inserted on top of the inner ring (by copying of the fraction of the inner ring and by recoloring it) to highlight the key enrichment groups based on their identification in the WT group treated with siRNA-LNP. Therefore, the inner ring that stems from MonaGO reflects the significance of the enrichment of a certain group of proteins as reflected by the scale of *p* values provided below the figure, whereas the protruding parts that appear as parts of the outer ring were inserted to help the reader in data interpretation. The color code of the outer ring is not related to enrichment. Heatmaps and hierarchical clustering analysis were made with Euclidean distance using the free Java-based tool Cluster 3.0 and clustering was visualized using Java Treeview 1.20 for generating heatmaps.

In order to identify proteins based on their regulation and significance via Volcano plots, this work used the output of the Spectronaut software and used the function “clear all filters”. In addition, the –Log₁₀ *p* value was calculated from the *p* value output and was used on the Y-axis, and the average Log₂ ratio from the output was used as X value. XY plots were drawn in Graph Pad prism 9. The cutoff data from Spectronaut for each data package (liver or serum samples) were used to display potential candidates shown in red color nodes. Blue coloring was assigned to some nodes to highlight selected proteins. Finally, significant regulation of individual proteins was calculated using relative protein abundance, normalized to the untreated WT control tissue, and shown as explained below.

RNA Sequencing of Liver Tissue: Total RNA from snap frozen pieces of liver tissue sizing about 5 mm was isolated using a Retch mill with metal beads for tissue homogenization. QiaShredders of an RNeasy Mini kit (Qi-

agen) were used to further purify the RNA according to the instructions of the manufacturer. RNase inhibitor ($20 \text{ U } \mu\text{L}^{-1}$) was used during RNA isolation (Applied Biosystems, Thermo Fisher Scientific, N8080119).

RNA quality control was done for all samples using a Bioanalyzer (Agilent) and sequencing was done using a Colibri 3' mRNA Library Prep Kit (Illumina). A NextSeq 500/550 High Output v2.5 kit was used. ERCC RNA Spike-in Mix (Thermo Fisher) was employed. The generation of the FASTQ files was done by bcl2fastq (Illumina). A reproducible analysis was achieved by sample processing with the publicly available nf-core/RNA-seq pipeline version 3.5 implemented in Nextflow 21.10.6 using Docker 20.10.12 using the minimal command. In brief, lane-level reads were trimmed using Trim Galore 0.6.7 and aligned to the mouse genome (GRCm39) using STAR 2.7.9a. Read mapping to a composite genome was made by concatenating the reference genome and 92 ERCC ExFold RNA Spike-In Mixes sequences (Thermo Fisher). Quantification of the levels of genes and transcripts was made by Salmon v1.5.2. All analyses were exerted by custom scripts in R 4.1.1 and by using the DESeq2 v1.32.0 framework. RNA seq data availability is provided in the Data availability statement.

Statistical Analysis: There was no preprocessing of imaging and flow cytometric data, proteomics data preprocessing was done as described in the methods above, and RNA seq data were also preprocessed as described in the respective sections. The data are expressed as the mean and standard error of the mean. The sample sizes are shown below each figure for each experimental group. Differences between groups with $*p < 0.05$, $**p < 0.01$, $***p < 0.001$ were considered significant. One way ANOVA was used for multiple group comparisons. Statistical analysis of data was exerted using GraphPad Prism 9.0 (GraphPad software, La Jolla, USA).

Data Availability Statement

The proteomics data have been deposited to the ProteomeXchange Consortium via the PRIDE partner repository.^[47] The dataset identifier is PXD032311. Password: qtbDmkM0. The targeted mass spectrometry proteomics data have been deposited to the PASSEL server with the data identifier PASS01743 (the data can be accessed using the following information: Username: PASS01743; Password: QH8557yy). RNA seq data were deposited to GEO (Record GSE213112; Token: wfgrycqcjfbjmr).

Supporting Information

Supporting Information is available from the Wiley Online Library or from the author.

Acknowledgements

C.L., A.M. contributed equally to this work. The authors thank Prof. Gabriele Zwadlo-Klarwasser and Dr. Elisa Brandt for helpful discussions. The authors are grateful to Diana Möckel for help with mouse experiments. This work was supported by the Genomics Facility, a core facility of the Interdisciplinary Center for Clinical Research (IZKF) Aachen within the Faculty of Medicine at RWTH Aachen University in Germany. This study was supported by the German Research Foundation (DFG) [BA6226/2-1, to M.B.]; the Wilhelm Sander Foundation [2018.129.1, to M.B.]; the COST Action Mye-InfoBank [CA20117, to M.B.]; a BMBF grant [16LW0143, to M.B.]; a GERLS long term stipend ID 91527866 [to A.M.]; a CSC stipend [202008320329, to C.L.]; a grant from the Interdisciplinary Center for Clinical Research within the faculty of Medicine at the RWTH Aachen University, the DZHK (German Centre for Cardiovascular Research), and the BMBF (German Ministry of Education and Research), NWO-ZonMw Veni 891619053 [to E.P.C.v.d.V.].

After initial online publication, Figure S1 was replaced on February 1, 2023. This was due to a previous error in the labeling of the images. This does not affect the overall results and conclusions of this work.

Open access funding enabled and organized by Projekt DEAL.

Conflict of Interest

The authors declare no conflict of interest.

Data Availability Statement

The data that support the findings of this study are available in the supplementary material of this article.

Keywords

hepatocytes, immune cells, imaging of siRNA-LNP, in vivo imaging, proteomics, siRNA-LNP, transcriptomics

Received: October 16, 2022

Revised: December 15, 2022

Published online:

- [1] U. Sahin, A. Muik, E. Derhovanessian, I. Vogler, L. M. Kranz, M. Vormehr, A. Baum, K. Pascal, J. Quandt, D. Maurus, S. Brachtendorf, V. Lork, J. Sikorski, R. Hilker, D. Becker, A. K. Eller, J. Grutzner, C. Boesler, C. Rosenbaum, M. C. Kuhnle, U. Luxemburger, A. Kemmer-Bruck, D. Langer, M. Bexon, S. Bolte, K. Kariko, T. Palanche, B. Fischer, A. Schultz, P. Y. Shi, et al., *Nature* **2020**, 586, 594.
- [2] A. Akinc, M. A. Maier, M. Manoharan, K. Fitzgerald, M. Jayaraman, S. Barros, S. Ansell, X. Du, M. J. Hope, T. D. Madden, B. L. Mui, S. C. Semple, Y. K. Tam, M. Ciufolini, D. Witzigmann, J. A. Kulkarni, R. van der Meel, P. R. Cullis, *Nat. Nanotechnol.* **2019**, 14, 1084.
- [3] A. Akinc, W. Querbes, S. De, J. Qin, M. Frank-Kamenetsky, K. N. Jayaprakash, M. Jayaraman, K. G. Rajeev, W. L. Cantley, J. R. Dorkin, J. S. Butler, L. Qin, T. Racie, A. Sprague, E. Fava, A. Zeigerer, M. J. Hope, M. Zerial, D. W. Sah, K. Fitzgerald, M. A. Tracy, M. Manoharan, V. Kotliansky, A. Fougerolles, M. A. Maier, *Mol. Ther.* **2010**, 18, 1357.
- [4] M. Dieckmann, M. F. Dietrich, J. Herz, *Biol. Chem.* **2010**, 391, 1341.
- [5] S. B. Azimifar, N. Nagaraj, J. Cox, M. Mann, *Cell Metab.* **2014**, 20, 1076.
- [6] K. Vercauteren, N. Van Den Eede, A. A. Mesalam, S. Belouard, M. T. Catanese, D. Bankwitz, F. Wong-Staal, R. Cortese, J. Dubuisson, C. M. Rice, T. Pietschmann, G. Leroux-Roels, A. Nicosia, P. Meuleman, *Hepatology* **2014**, 60, 1508.
- [7] T. J. Nieland, J. T. Shaw, F. A. Jaipuri, J. L. Duffner, A. N. Koehler, S. Banakos, V. I. Zannis, T. Kirchhausen, M. Krieger, *Biochemistry* **2008**, 47, 460.
- [8] K. R. Feingold, C. Grunfeld, in *Introduction to Lipids and Lipoproteins*. (Eds: K. R. Feingold, B. Anawalt, A. Boyce, G. Chrousos, W. W. de Herder, K. Dhatariya, K. Dungan, J. M. Hershman, J. Hoffland, S. Kalra, G. Kaltsas, C. Koch, P. Kopp, M. Korbonits, C. S. Kovacs, W. Kuohung, B. Laferriere, M. Levy, E. A. McGee, R. McLachlan, J. E. Morley, M. New, J. Purnell, R. Sahay, F. Singer, M. A. Sperling, C. A. Stratakis, D. L. Trencle, D. P. Wilson), MDText.com, Inc., South Dartmouth, MA **2000**.
- [9] a) F. Sasaki, T. Koga, M. Ohba, K. Saeki, T. Okuno, K. Ishikawa, T. Nakama, S. Nakao, S. Yoshida, T. Ishibashi, H. Ahmadi, M. R. Kanavi, A. Hafezi-Moghadam, J. M. Penninger, K. H. Sonoda, T. Yokomizo, *JCI Insight* **2018**, 3, 30232269; b) K. Kojo, Y. Ito, K. Eshima, N. Nishizawa, H. Ohkubo, T. Yokomizo, T. Shimizu, M. Watanabe, M. Majima, *Sci. Rep.* **2016**, 6, 29650; c) F. Okamoto, K. Saeki, H. Sumimoto, S. Yamasaki, T. Yokomizo, *J. Biol. Chem.* **2010**, 285, 41113.
- [10] J. Lv, Y. Xiong, W. Li, W. Yang, L. Zhao, R. He, *J. Immunol.* **2017**, 198, 1673.
- [11] a) M. Bartneck, T. Ritz, H. A. Keul, M. Wambach, J. Bornemann, U. Gbureck, J. Ehling, T. Lammers, F. Heymann, N. Gassler, T. Ludde, C. Trautwein, J. Groll, F. Tacke, *ACS Nano* **2012**, 6, 8767; b) M. Bartneck, K. M. Scheyda, K. T. Warzecha, L. Y. Rizzo, K. Hittatiya, T. Luedde, G. Storm, C. Trautwein, T. Lammers, F. Tacke, *Biomaterials* **2015**, 37, 367;

- c) M. Bartneck, C. T. Schlosser, M. Barz, R. Zentel, C. Trautwein, T. Lammers, F. Tacke, *ACS Nano* **2017**, *11*, 9689.
- [12] O. Krenkel, F. Tacke, *Nat. Rev. Immunol.* **2017**, *17*, 306.
- [13] A. C. C. Vieira, L. L. Chaves, M. Pinheiro, S. A. C. Lima, D. Ferreira, B. Sarmento, S. Reis, *Artif. Cells, Nanomed., Biotechnol.* **2018**, *46*, 653.
- [14] N. Veiga, M. Goldsmith, Y. Granot, D. Rosenblum, N. Dammes, R. Kedmi, S. Ramishetti, D. Peer, *Nat. Commun.* **2018**, *9*, 4493.
- [15] R. Kedmi, N. Veiga, S. Ramishetti, M. Goldsmith, D. Rosenblum, N. Dammes, I. Hazan-Halevy, L. Nahary, S. Leviatan-Ben-Arye, M. Harlev, M. Behlke, I. Benhar, J. Lieberman, D. Peer, *Nat. Nanotechnol.* **2018**, *13*, 214.
- [16] H. M. Miettinen, J. M. Gripenroeg, C. I. Lord, J. O. Nagy, *PLoS One* **2018**, *13*, e0200444.
- [17] R. Pattipeiluhu, G. Arias-Alpizar, G. Basha, K. Y. T. Chan, J. Bussmann, T. H. Sharp, M. A. Moradi, N. Sommerdijk, E. N. Harris, P. R. Cullis, A. Kros, D. Witzigmann, F. Campbell, *Adv. Mater.* **2022**, *34*, 2201095.
- [18] G. Basha, T. I. Novobrantseva, N. Rosin, Y. Y. Tam, I. M. Hafez, M. K. Wong, T. Sugo, V. M. Ruda, J. Qin, B. Klebanov, M. Ciufolini, A. Akinc, Y. K. Tam, M. J. Hope, P. R. Cullis, *Mol. Ther.* **2011**, *19*, 2186.
- [19] D. Szklarczyk, A. L. Gable, K. C. Nastou, D. Lyon, R. Kirsch, S. Pyysalo, N. T. Doncheva, M. Legeay, T. Fang, P. Bork, L. J. Jensen, C. von Merling, *Nucleic Acids Res.* **2021**, *49*, D605.
- [20] B. P. Smith, L. S. Auvil, M. Welge, C. B. Bushnell, R. Bhargava, N. Elango, K. Johnson, Z. Madak-Erdogan, *Sci. Rep.* **2020**, *10*, 19128.
- [21] T. Yokomizo, *J. Biochem.* **2015**, *157*, 65.
- [22] M. Kato, S. Khan, E. d'Aniello, K. J. McDonald, D. N. Hart, *J. Immunol.* **2007**, *179*, 6052.
- [23] Y. S. Roh, B. Zhang, R. Loomba, E. Seki, *Am. J. Physiol.: Gastrointest. Liver Physiol.* **2015**, *309*, G30.
- [24] Y. Saiman, S. L. Friedman, *Front. Physiol.* **2012**, *3*, 213.
- [25] H. Sahin, E. Borkham-Kamphorst, C. Kuppe, M. M. Zaldivar, C. Grouls, M. Al-samman, A. Nellen, P. Schmitz, D. Heinrichs, M. L. Berres, D. Doleschel, D. Scholten, R. Weiskirchen, M. J. Moeller, F. Kiessling, C. Trautwein, H. E. Wasmuth, *Hepatology* **2012**, *55*, 1610.
- [26] H. Ni, M. Z. C. Hatit, K. Zhao, D. Loughrey, M. P. Lokugamage, H. E. Peck, A. D. Cid, A. Muralidharan, Y. Kim, P. J. Santangelo, J. E. Dahlman, *Nat. Commun.* **2022**, *13*, 4766.
- [27] S. S. Yu, C. M. Lau, W. J. Barham, H. M. Onishko, C. E. Nelson, H. Li, C. A. Smith, F. E. Yull, C. L. Duvall, T. D. Giorgio, *Mol. Pharm.* **2013**, *10*, 975.
- [28] F. Ginhoux, S. Jung, *Nat. Rev. Immunol.* **2014**, *14*, 392.
- [29] A. J. Da Silva Sanchez, C. Dobrowolski, A. Cristian, E. S. Echeverri, K. Zhao, M. Z. C. Hatit, D. Loughrey, K. Paunovska, J. E. Dahlman, *Nano Lett.* **2022**, *22*, 4822.
- [30] M. S. Spagnuolo, B. Maresca, V. L. a Marca, A. Carrizzo, C. Veronesi, C. Cupidi, T. Piccoli, R. G. Maletta, A. C. Bruni, P. Abrescia, L. Cigliano, *ACS Chem. Neurosci.* **2014**, *5*, 837.
- [31] N. Katoh, H. Nakagawa, *J. Vet. Med. Sci.* **1999**, *61*, 119.
- [32] A. L. Barran-Berdon, D. Pozzi, G. Caracciolo, A. L. Capriotti, G. Caruso, C. Cavaliere, A. Riccioli, S. Palchetti, A. Lagana, *Langmuir* **2013**, *29*, 6485.
- [33] D. J. Hogan, D. P. Riordan, A. P. Gerber, D. Herschlag, P. O. Brown, *PLoS Biol.* **2008**, *6*, e255.
- [34] V. Fensterl, C. S. Ganes, *J. Interferon Cytokine Res.* **2011**, *31*, 71.
- [35] A. Ji, X. Wang, V. P. Noffsinger, D. Jennings, M. C. de Beer, F. C. de Beer, L. R. Tannock, N. R. Webb, *J. Lipid Res.* **2020**, *61*, 328.
- [36] The UniProt Consortium, *Nucleic Acids Res.* **2016**, *45*, D158.
- [37] N. Gamage, A. Barnett, N. Hempel, R. G. Duggleby, K. F. Windmill, J. L. Martin, M. E. McManus, *Toxicol. Sci.* **2005**, *90*, 5.
- [38] C. K. Elechalawar, M. N. Hossen, L. McNally, R. Bhattacharya, P. Mukherjee, *J. Controlled Release* **2020**, *322*, 122.
- [39] W. Lai, D. Li, Q. Wang, X. Nan, Z. Xiang, Y. Ma, Y. Liu, J. Chen, J. Tian, Q. Fang, *Int. J. Nanomed.* **2020**, *15*, 1481.
- [40] A. Amici, G. Caracciolo, L. Digiacomo, V. Gambini, C. Marchini, M. Tilio, A. L. Capriotti, V. Colapicchioni, R. Matassa, G. Familiari, S. Palchetti, D. Pozzi, M. Mahmoudi, A. Laganà, *RSC Adv.* **2017**, *7*, 1137.
- [41] S. Ishibashi, M. S. Brown, J. L. Goldstein, R. D. Gerard, R. E. Hammer, J. Herz, *J. Clin. Invest.* **1993**, *92*, 883.
- [42] M. Lino, S. Farr, C. Baker, M. Fuller, B. Trigatti, K. Adeli, *Am. J. Physiol.* **2015**, *309*, G350.
- [43] A. Fedoseenko, M. Wijers, J. C. Wolters, D. Dekker, M. Smit, N. Huijckman, N. Kloosterhuis, H. Klug, A. Schepers, K. Willems van Dijk, J. H. M. Levels, D. D. Billadeau, M. H. Hofker, J. van Deursen, M. Westerterp, E. Burstein, J. A. Kuivenhoven, B. van de Sluis, *Circ. Res.* **2018**, *122*, 1648.
- [44] A. B. Wegrzyn, K. Herzog, A. Gerding, M. Kwiatkowski, J. C. Wolters, A. M. Dolga, A. E. M. van Lint, R. J. A. Wanders, H. R. Waterham, B. M. Bakker, *FEBS J.* **2020**, *287*, 5096.
- [45] J. C. Wolters, J. Ciapaite, K. van Eunen, K. E. Niezen-Koning, A. Matton, R. J. Porte, P. Horvatovich, B. M. Bakker, R. Bischoff, H. P. Permentier, *J. Proteome Res.* **2016**, *15*, 3204.
- [46] Z. Xin, Y. Cai, L. T. Dang, H. M. S. Burke, J. Revote, N. Charitakis, D. Bienroth, H. T. Nim, Y. F. Li, M. Ramialison, *BMC Bioinformatics* **2022**, *23*, 69.
- [47] Y. Perez-Riverol, J. Bai, C. Bandla, D. Garcia-Seisdedos, S. Hewapathirana, S. Kamatchinathan, D. J. Kundu, A. Prakash, A. Frericks-Zipper, M. Eisenacher, M. Walzer, S. Wang, A. Brazma, J. A. Vizcaino, *Nucleic Acids Res.* **2022**, *50*, D543.